9444 *Inorg. Chem.* **2009**, *48*, 9444–9453
DOI: 10.1021/ic9013366

Inorganic Chemistry
Article

Ruthenium(II) Arene Anticancer Complexes with Redox-Active Diamine Ligands

Tijana Bugarcic,[†,‡] Abraha Habtemariam,[‡] Robert J. Deeth,[‡] Francesca P. A. Fabbiani,[†] Simon Parsons,[†] and Peter J. Sadler*[,‡]

[†]*School of Chemistry, University of Edinburgh, West Mains Road, Edinburgh EH9 3JJ, U.K., and*
[‡]*Department of Chemistry, University of Warwick, Coventry CV4 7AL, U.K.*

Received July 10, 2009

The synthesis and characterization of ruthenium(II) arene complexes of the general formula $[(\eta^6\text{-arene})Ru(XY)Z]^+$, where arene = *p*-cymene (*p*-cym), hexamethylbenzene (hmb), or biphenyl (bip), XY = *o*-phenylenediamine (*o*-pda), *o*-benzoquinonediimine (*o*-bqdi), or 4,5-dimethyl-*o*-phenylenediamine (dmpda), and Z = Cl, Br, or I, are reported (complexes **1**−**6**). In addition, the X-ray crystal structures of $[(\eta^6\text{-}p\text{-cym})Ru(o\text{-pda})Cl]PF_6$ (**1**) and $[(\eta^6\text{-hmb})Ru(o\text{-bqdi})Cl]PF_6$ (**3PF$_6$**) are described. The Ru−N distances in **3PF$_6$** are significantly shorter [2.033(4) and 2.025(4) Å] compared to those in **1** [2.141(2) and 2.156(2) Å]. All of the imine complexes (**3**−**5**) exhibit a characteristic broad ^{1}H NMR NH resonance at ca. δ 14−15. Complex **1** undergoes concomitant ligand-based oxidation and hydrolysis (38% after 24 h) in water. The oxidation also occurs in methanol. The iodido complex $[(\eta^6\text{-}p\text{-cym})Ru(o\text{-bqdi})I]I$ (**4**) did not undergo hydrolysis, whereas the chlorido complex **3** showed relatively fast hydrolysis ($t_{1/2}$ = 7.5 min). Density functional theory calculations showed that the total bonding energy of 9-EtG in $[(\eta^6\text{-}p\text{-cym})Ru(o\text{-pda})(9\text{-EtG-}N7)]^{2+}$ (**1EtG**) is 23.8 kJ/mol lower than that in $[(\eta^6\text{-}p\text{-cym})Ru(o\text{-bqdi})(9\text{-EtG-}N7)]^{2+}$ (**3EtG**). The greater bonding energy is related to the contribution from strong hydrogen bonding between the NH proton of the chelating ligand and O6 of 9-EtG (1.69 Å). A loss of cytotoxic activity was observed upon oxidation of the amine ligand to an imine (e.g., IC_{50} = 11 μM for **1** and IC_{50} > 100 μM for **3**, against A2780 ovarian cancer cells). The relationship between the cytotoxic activity and the solution and solid state structures of the imine and amine complexes is discussed.

Introduction

Ruthenium complexes have potential as anticancer agents.[1] Two Ru^{III} complexes are in clinical trials: *trans*-$[Ru^{III}(dmso)(Im)Cl_4][ImH]$ (Nami-A; Im = imidazole)[2] and *trans*-$[Ru^{III}(Ind)_2Cl_4][IndH]$ (KP1019; Ind = indazole).[3] Their proposed mode of action involves the in vivo reduction of Ru^{III} to the more reactive Ru^{II}.[1,4] Organoruthenium complexes of the type $[(\eta^6\text{-arene})Ru^{II}(en)Cl]^+$, where the arene is benzene or a benzene derivative, and en = ethylenediamine exhibit anticancer activity, including activity against cisplatin-resistant cancer cells.[5,6] In this type of complex, the arene provides a hydrophobic face and the cytotoxicity increases with the size of the arene.[5] The arene stabilizes ruthenium in the 2+ oxidation state so that oxidation to Ru^{III} is difficult. Hydrolysis of the Ru−Cl bond appears to be important for activation, giving the aqua adduct $[(\eta^6\text{-arene})Ru^{II}(en)H_2O]^{2+}$, which can bind to DNA and form a monofunctional adduct. The chelating ligand provides additional stability. The nature of the chelating ligand can play a crucial role in anticancer activity.[7] In this work, we have investigated complexes in which the chelating ligand is a phenylenediamine.

Transition-metal complexes with *o*-phenylenediamine (*o*-pda) as a chelating ligand are of particular interest because of their redox properties. Dichloridoplatinum(II) complexes containing *o*-pda were among the first cisplatin analogues to exhibit antitumor activity.[8−10] Recently, good activity for Ru^{II}(*o*-pda) complexes of the type $[(\eta^6\text{-arene})Ru^{II}(o\text{-pda})Cl]^+$, containing a range of mono-, di-, and tricyclic hydrocarbons

*To whom correspondence should be addressed. E-mail: P.J.Sadler@warwick.ac.uk.

(1) Clarke, M. J.; Zhu, F.; Frasca, D. R. *Chem. Rev.* **1999**, *99*, 2511–2533.
(2) Sava, G.; Alessio, E.; Bergamo, A.; Mestroni, G. *Top. Biol. Inorg. Chem.* **1999**, *1*, 143–169.
(3) Galanski, M.; Arion, V. B.; Jakupec, M. A.; Keppler, B. K. *Curr. Pharm. Des.* **2003**, *9*, 2078–2089.
(4) Clarke, M. J.; Bitler, S.; Rennert, D.; Buchbinder, M.; Kelman, A. D. *J. Inorg. Biochem.* **1980**, *12*, 79–87.
(5) Aird, R. E.; Cummings, J.; Ritchie, A. A.; Muir, M.; Morris, R. E.; Chen, H.; Sadler, P. J.; Jodrell, D. I. *Br. J. Cancer* **2002**, *86*, 1652–1657.
(6) Morris, R. E.; Aird, R. E.; Murdoch, P. d. S.; Chen, H.; Cummings, J.; Hughes, N. D.; Parsons, S.; Parkin, A.; Boyd, G.; Jodrell, D. I.; Sadler, P. J. *J. Med. Chem.* **2001**, *44*, 3616–3621.
(7) Habtemariam, A.; Melchart, M.; Fernandez, R.; Parsons, S.; Oswald, I. D. H.; Parkin, A.; Fabbiani, F. P. A.; Davidson, J. E.; Dawson, A.; Aird, R. E.; Jodrell, D. I.; Sadler, P. J. *J. Med. Chem.* **2006**, *49*, 6858–6868.
(8) Connors, T. A.; Jones, M.; Ross, W. C.; Braddock, P. D.; Khokhar, A. R.; Tobe, M. L. *Chem. Biol. Interact.* **1972**, *5*, 415–424.
(9) Gale, G. R.; Atkins, L. M.; Walker, E. M., Jr.; Smith, A. B.; Meischen, S. J. *Proc. Soc. Exp. Biol. Med.* **1973**, *142*, 1349–1354.
(10) Meischen, S. J.; Gale, G. R.; Lake, L. M.; Frangakis, C. J.; Rosenblum, M. G.; Walker, E. M., Jr.; Atkins, L. M.; Smith, A. B. *J. Nat. Cancer Inst.* **1976**, *57*, 841–845.

 Published on Web 09/08/2009

(arenes), has been reported.[7] Complexes containing mono- or dimethylated *o*-pda and indan as the arene also exhibit good activity. The incorporation of OH groups onto the chelating ligand (*o*-pda) decreases the activity. It has been found that these complexes have the ability to overcome cross-resistance toward adriamycin (doxorubicin). The reduction in the resistance factor (RF), where RF = $IC_{50}(A2780^{AD})/IC_{50}(A2780)$, achievable by replacing en by *o*-pda, can be dramatic. For $[(\eta^6\text{-tha})Ru^{II}(en)Cl]^+$, where tha = tetrahydroanthracene, RF reduces from >100 to 2 when en is replaced with *o*-pda to form $[(\eta^6\text{-tha})Ru^{II}(o\text{-pda})Cl]^+$ and from 92 to 2 for the analogous dihydroanthracene (dha) complex.

In this paper, we report the preparation and characterization of six ruthenium(II) arene complexes containing *o*-pda, *o*-benzoquinonediimine (*o*-bqdi), or 4,5-dimethyl-*o*-phenylenediamine (dmpda) as chelating ligands, with a variety of arenes and halides as the remaining ligands. The effect of the variation of the arene and halides on the oxidation of coordinated *o*-pda, as well as their effect on cytotoxicity against A2780 human ovarian and A549 human lung cancer cell lines, was investigated. We have compared the aqueous solution chemistry of complexes containing *o*-pda and its oxidized form *o*-bqdi. The difference in the solid-state structures of the diamine and diimine complexes is investigated. The X-ray crystal structures of complexes $[(\eta^6\text{-}p\text{-cym})Ru(o\text{-pda})Cl]PF_6$ (**1**; *p*-cym = *p*-cymene) and $[(\eta^6\text{-hmb})Ru(o\text{-bqdi})Cl]]PF_6$ (**3**; hmb = hexamethylbenzene) are reported. The stability of 9-EtG adducts of complexes **1** and **3** is studied using density functional theory (DFT) calculations. The ability of the diimine complex $[(\eta^6\text{-}p\text{-cym})Ru(o\text{-bqdi})I]^+$ (**4**) to undergo ligand-based reduction by glutathione (GSH) in water to give the diamine complex $[(\eta^6\text{-}p\text{-cym})Ru(o\text{-pda})I]^+$ (**8**) has also been investigated.

Experimental Section

Materials. The starting materials $[(\eta^6\text{-arene})RuX_2]_2$ [X = Cl or I and arene = *p*-cymene (*p*-cym), hexamethylbenzene (hmb), and biphenyl (bip)] were prepared according to literature methods.[11,12] *o*-Phenylenediamine (*o*-pda) and 4,5-dimethyl-*o*-phenylenediamine (dmpda) were purchased from Sigma-Aldrich and glutathione (GSH) from Acros Organics. Ethanol and methanol were dried over Mg/I_2.

Synthesis of Ruthenium Complexes. Complexes **1**−**4** and **6** were synthesized using a similar procedure. Typically, the ligand, *o*-pda or dmpda (2 mol equiv), was added to a methanolic solution of the ruthenium dimer $[(\eta^6\text{-arene})RuCl_2]_2$ and the reaction mixture stirred at ambient temperature for 30 min. Iodido and bromido complexes **4** and **5** were synthesized in the halide exchange reaction, using the chlorido complex **1** and ca. 5 mol equiv of KX (X = I or Br). The products were isolated as PF_6, Cl, or I salts. The details for individual reactions are described below.

$[(\eta^6\text{-}p\text{-cym})Ru(o\text{-pda})Cl]PF_6$ (1). To a suspension of $[(\eta^6\text{-}p\text{-cym})RuCl_2]_2$ (0.05 g, 0.08 mmol) in dry, freshly distilled methanol (30 mL) was added *o*-pda (0.02 g, 0.16 mmol). The reaction mixture turned yellow immediately after the addition of *o*-pda. It was stirred at ambient temperature in air for 30 min. The clear yellow solution was filtered, NH_4PF_6 (0.06 g, 0.40 mmol) added, and the flask shaken. A precipitate started to appear almost immediately. The fine yellow precipitate was collected by filtration, washed with cold methanol and ether, and dried in air. Yield: 89%.

(11) Zelonka, R. A.; Baird, M. C. *Can. J. Chem.* **1972**, *50*, 3063–3072.
(12) Beasley, T. J.; Brost, R. D.; Chu, C. K.; Grundy, S. L.; Stobart, S. R. *Organometallics* **1993**, *12*, 4599–4606.

Crystals of $[(\eta^6\text{-}p\text{-cym})Ru(o\text{-pda})Cl]PF_6$ suitable for X-ray analysis were obtained by the slow evaporation of a methanolic solution at ambient temperature. ESI-MS. Calcd for $C_{16}H_{22}ClN_2Ru^+$ $[M]^+$: *m*/*z* 378.9. Found: *m*/*z* 379.1. Anal. Calcd for $C_{16}H_{22}ClF_6N_2PRu$ (**1**): C, 36.68; H, 4.23; N, 5.35. Found: C, 36.56; H, 4.16; N, 5.32. ^1H NMR in DMSO-d_6: δ 8.01 (d, 2H, NH), 7.21 (m, 4H), 6.34 (d, 2H, NH), 5.75 (d, 2H), 5.52 (d, 2H), 2.28 (m, 1H), 2.21 (s, 3H), 1.18 (d, 6H).

$[(\eta^6\text{-hmb})Ru(o\text{-pda})Cl]PF_6$ (2). To a suspension of $[(\eta^6\text{-hmb})RuCl_2]_2$ (0.05 g, 0.07 mmol) in dry, freshly distilled methanol (30 mL) was added *o*-pda (0.02 g, 0.15 mmol). The reaction mixture was stirred at ambient temperature under argon for 30 min. The resultant red solution was filtered, NH_4PF_6 (0.06 g, 0.39 mmol) added, and the flask shaken. A precipitate started to appear almost immediately. The precipitate was collected by filtration, washed with cold methanol and ether, and dried in air to give a red solid. Yield: 73%.

The analysis suggested that the product contained a mixture of counteranions. Anal. Calcd for a 4:1 PF_6/Cl mixture of $C_{18}H_{26}ClF_6N_2PRu$ and $C_{18}H_{26}Cl_2N_2Ru$: C, 40.79; H, 4.94; N, 5.28. Found: C, 40.91; H, 4.34; N, 5.59. ^1H NMR in DMSO-d_6: δ 7.11 (m, 4H), 6.71 (d, 2H, NH), 6.51 (d, 2H, NH), 2.01 (s, 18H).

$[(\eta^6\text{-hmb})Ru(o\text{-bqdi})Cl]Cl$ (3). To a suspension of $[(\eta^6\text{-hmb})RuCl_2]_2$ (0.05 g, 0.07 mmol) in dry, freshly distilled methanol (30 mL) was added *o*-pda (0.02 g, 0.15 mmol). The reaction mixture was stirred at ambient temperature in air for 30 min. The solvent was removed under reduced pressure to leave a solid. A small amount of the solid was taken for ^1H NMR analysis in DMSO-d_6, which showed a mixture of complexes **2** and **3** in a ratio 1:1. The remaining solid was redissolved in methanol and left in air overnight. The purple solid that formed was collected by filtration, washed with cold methanol, followed by ether, and dried in air. Yield: 67%.

Anal. Calcd for $C_{18}H_{24}Cl_2N_2Ru$ (**3**): C, 49.09; H, 5.49; N, 6.36. Found: C, 48.50; H, 5.83; N, 5.79. ESI-MS. Calcd for $C_{18}H_{24}ClN_2Ru^+$ $[M]^+$: *m*/*z* 404.9. Found: *m*/*z* 405.1. ^1H NMR in DMSO-d_6: δ 13.97 (s, 2H, NH), 7.11 (m, 4H), 2.03 (s, 18H).

Crystals of $[(\eta^6\text{-hmb})Ru(o\text{-bqdi})Cl]PF_6$ (**3PF$_6$**) suitable for X-ray analysis were obtained by dissolution of complex **3** in methanol followed by the addition of NH_4PF_6 (0.06 g, 0.39 mmol) and evaporation of the solvent slowly at ambient temperature.

$[(\eta^6\text{-}p\text{-cym})Ru(o\text{-bqdi})I]I$ (4). Two methods were used in the preparation of **4**.

Method A: To a suspension of $[(\eta^6\text{-}p\text{-cym})RuI_2]_2$ (0.05 g, 0.05 mmol) in dry, freshly distilled methanol (30 mL) was added *o*-pda (0.01 g, 0.10 mmol). The reaction mixture turned purple immediately. It was stirred at ambient temperature in air for 30 min. The clear dark-purple solution was filtered and left overnight at ambient temperature to allow the solvent to evaporate. The precipitate that appeared was collected by filtration, washed with cold methanol and ether, and dried in air to give a dark-purple solid. Yield: 73%.

Method B: To a suspension of complex **1** (0.01 g, 0.02 mmol) in dry, freshly distilled methanol (30 mL) was added KI (0.02 g, 0.09 mmol). The reaction mixture was stirred at ambient temperature in air for 30 min. The yellow solution turned dark purple, and a dark-purple precipitate appeared. The precipitate was collected by filtration, washed with cold methanol and ether, and dried in air to give a dark-purple solid. Yield: 36%.

Anal. Calcd for $C_{16}H_{20}I_2N_2Ru$ (**4**): C, 32.29; H, 3.36; N, 4.71. Found: C, 32.59; H, 3.99; N, 5.41. ESI-MS. Calcd for $C_{16}H_{20}IN_2Ru^+$ $[M]^+$: *m*/*z* 468.3. Found: *m*/*z* 468.9. ^1H NMR in DMSO-d_6: δ 14.68 (s, 2H, NH), 7.09 (m, 4H), 6.33 (d, 2H), 6.11 (d, 2H), 2.95 (m, 1H), 2.43 (s, 3H), 1.20 (d, 6H).

$[(\eta^6\text{-}p\text{-cym})Ru(o\text{-bqdi})Br]PF_6$ (5). To a suspension of complex **1** (0.01 g, 0.02 mmol) in dry, freshly distilled methanol (30 mL) was added KBr (0.01 g, 0.12 mmol). The reaction mixture was stirred at ambient temperature in air for 30 min. The yellow

solution turned purple, and a dark-purple precipitate started to appear. The dark-purple precipitate was collected by filtration, washed with cold methanol and ether, and dried in air. Yield: 32%.

ESI-MS. Calcd for $C_{16}H_{20}BrN_2Ru^+$ $[M]^+$: m/z 421.3. Found: m/z 421.3. ^{1}H NMR in DMSO-d_6: δ 14.70 (s, 2H, NH), 7.08 (m, 4H), 6.30 (d, 2H), 6.07 (d, 2H), 2.87 (m, 1H), 2.33 (s, 3H), 1.19 (d, 6H).

[(η^6-bip)Ru(dmpda)Cl]PF_6 (6). To a suspension of [(η^6-bip)-$RuCl_2$]$_2$ (0.05 g, 0.08 mmol) in dry, freshly distilled methanol (30 mL) was added dmpda (0.02 g, 0.15 mmol). The reaction mixture was stirred at ambient temperature in air for 30 min. The dark-violet solution was filtered, NH_4PF_6 (0.06 g, 0.38 mmol) added, and the flask shaken. The precipitate that appeared almost immediately was collected by filtration, washed with cold methanol and ether, and dried in air to give a violet solid. Yield: 49%.

ESI-MS. Calcd for $C_{20}H_{22}ClN_2Ru^+$ $[M]^+$: m/z 426.9. Found: m/z 426.9. Anal. Calcd for $C_{20}H_{26}ClF_6N_2PO_2Ru$ (**6**·$2H_2O$): C, 39.51; H, 4.31; N, 4.61. Found: C, 39.11; H, 3.86; N, 4.44. ^{1}H NMR in DMSO-d_6: δ 8.20 (d, 2H, NH), 7.84 (d, 2H), 7.50 (m, 3H), 6.98 (s, 2H), 6.30 (d, 2H, NH), 6.26 (d, 2H), 6.00 (t, 1H), 5.88 (t, 2H), 2.15 (s, 6H).

NMR Spectroscopy. All NMR spectra were recorded on either Bruker DMX (500 MHz) or AVA (600 MHz) spectrometers. ^{1}H NMR signals were referenced to the residual solvent peak, δ 2.52 (DMSO) and δ 3.34 (methanol). For solutions in D_2O, dioxane was used as an internal reference (δ 3.75). All spectra were recorded at 298 K unless stated otherwise, using 5 mm diameter tubes. The data were processed using XWIN-NMR (version 3.6; Bruker UK Ltd.).

Elemental Analysis. Elemental analyses were carried out by the Warwick Analytical Service or by the University of Edinburgh, using an Exeter CE 440 analytical analyzer.

Electrospray Ionization Mass Spectrometry (ESI-MS). Positive-ion ESI-MS spectra were obtained on a Micromass Platform II mass spectrometer, and solutions were infused directly. The capillary voltage was 3.5 V, and the cone voltage was 25 V. The source temperature was dependent on the solvent used. Data were collected and analyzed on a MASS LYNX V3.5 Windows NT PC data system.

X-ray Crystallography. Diffraction data for compounds **1** and **3PF$_6$** were collected at 150 K using a Bruker Smart Apex CCD diffractometer. Absorption corrections for all data sets were performed with the multiscan procedure *SADABS*.[13] The structure of **3PF$_6$** was solved by direct methods (*SIR92*)[14] and that of **1** by Patterson methods (*DIRDIF*).[15] Refinement was against F^2 using all data (*CRYSTALS* for **3PF$_6$** and *SHELXTL* for **1**).[16] Hydrogen atoms attached to nitrogen were found in difference maps, and the pattern of hydrogen bonding in the two structures is consistent with the positions suggested. All non-hydrogen atoms were refined with anisotropic displacement parameters. The programs *Diamond 3.020*,[17] *Mercury 1.4.1*,[18] and *ORTEP 32*[19] were used for the analysis of data and production of graphics.

The crystal structures of **1** and **3PF$_6$** have been deposited in the Cambridge Crystallographic Data Center under accession numbers CCDC 714902 and 714903, respectively, and are available in the Supporting Information.

UV−vis Spectroscopy. A Perkin-Elmer Lambda-16 UV−vis spectrophotometer was used with quartz cuvettes (1 cm path length; 0.5 mL) and a PTP1 Peltier temperature controller. Experiments were carried out at 298 K unless otherwise stated.

Hydrolyses. Hydrolyses of chloridoruthenium(II) arene complexes were monitored by UV−vis spectroscopy. Complexes were dissolved in water, rapidly prior to recording the first spectrum, to give ca. 50 μM solutions. The absorbance was recorded at 30 s intervals at selected wavelengths over ca. 30 min at 310 K. Plots of the change in absorbance with time were fitted to the appropriate equation for pseudo-first-order kinetics using *Origin*, version 7.5 (Microcal Software Ltd.), to give the half-lives and rate constants.

Oxidation in Methanol. The oxidation of complex **1** was monitored in methanol (50 μM solution) in the absence and in the presence of KI (1 mol equiv) by UV−vis spectroscopy. The absorbance was recorded at 30 s intervals at selected wavelengths over ca. 4 h at 310 K. Plots of the change in absorbance with time were fitted to the appropriate equation for pseudo-first-order kinetics using *Origin*, version 7.5 (Microcal Software Ltd.), to give the half-lives and rate constants.

Reaction with GSH. UV−vis spectra of complex **4** in water (50 μM), in the presence of 15 mol equiv of GSH, were recorded at 5 min intervals for 1 h at 310 K.

The ^{1}H NMR spectra of a D_2O solution of complex **4** (200 μM), in the presence of 15 mol equiv of GSH, were recorded 15 min, 2 h, 4 h, 24 h, and 72 h after dissolution at 310 K.

Computation. The 9-EtG adducts of complexes **1** and **3** (**1EtG** and **3EtG**, respectively) were created by substituting the chlorido ligand with 9-EtG in the crystal structures of **1** and **3** in *Chemcraft* (Version 1.5). The 9-EtG used in the substitution was imported into the database of *Chemcraft* from the previously determined X-ray crystal structure of the 9-EtG adduct of the ruthenium(II) arene complex similar in structure to complexes **1** and **3**. The coordinates used for the calculations were obtained directly from *ChemCraft*. The calculations were carried out using DFT with the generalized gradient approximation, as implemented in the Amsterdam density functional (ADF)[20] program (version 2007.01). Geometries and energies were obtained by using the Becke−Perdew gradient-corrected functional (BP86) with scalar ZORA relativistic correction,[21−25] unless otherwise stated. The general numerical integration was 4.0. The frozen-core approximation (small core)[26] was applied using triple-ζ plus polarization bases. Default convergence criteria were applied for self-consistent-field and geometry optimization. The conductor-like screening model, as implemented in ADF, was used to simulate the aqueous environment with ε = 78.4 and a probe radius = 1.9 Å. The atomic radii used were Ru = 1.950, Cl = 1.725, O = 1.517, N = 1.608, C = 1.700, and H = 1.350. Estimates of the Ru−9-EtG bonding energies in **1EtG** and **3EtG** were obtained by subtraction of the

(13) Sheldrick, G. M. *SADABS*, version 2006-1; University of Göttingen: Göttingen, Germany, **2006**.
(14) Altomare, A.; Cascarano, G.; Giacovazzo, C.; Guagliardi, A.; Burla, M. C.; Polidori, G.; Camalli, M. *J. Appl. Crystallogr.* **1994**, *27*, 435–435.
(15) Beurskens, P. T.; Beurskens, G.; Bosman, W. P.; de Gelder, R.; Garcia-Granda, S.; Gould, R. O.; Israel, R.; Smits, J. M. M. *The DIRDIF96 Program System*; University of Nijmegen: Nijmegen, The Netherlands, **1996**.
(16) Sheldrick, G. M. *SHELXL-97*; University of Göttingen, Göttingen, Germany, **1997**.
(17) *DIAMOND, Visual crystal structure information system*, version 3.0; Crystal Impact GbR: Bonn, Germany, 2004.
(18) Macrae, C. F.; Edgington, P. R.; McCabe, P.; Pidcock, E.; Shields, G. P.; Taylor, R.; Towler, M.; van de Streek, J. *J. Appl. Crystallogr.* **2006**, *39*, 453–457.
(19) Farrugia, L. J. *J. Appl. Crystallogr.* **1997**, *30*, 565.
(20) Te Velde, G.; Bickelhaupt, F. M.; Baerends, E. J.; Fonseca Guerra, C.; Van Gisbergen, S. J. A.; Snijders, J. G.; Ziegler, T. *J. Comput. Chem.* **2001**, *22*, 931–967.
(21) van Lenthe, E.; Baerends, E. J.; Snijders, J. G. *J. Chem. Phys.* **1993**, *99*, 4597–4610.
(22) van Lenthe, E.; Baerends, E. J.; Snijders, J. G. *J. Chem. Phys.* **1994**, *101*, 9783–9792.
(23) van Lenthe, E.; Ehlers, A.; Baerends, E. J. *J. Chem. Phys.* **1999**, *110*, 8943–8953.
(24) van Lenthe, E.; Snijders, J. G.; Baerends, E. J. *J. Chem. Phys.* **1996**, *105*, 6505–6516.
(25) van Lenthe, E.; Van Leeuwen, R.; Baerends, E. J.; Snijders, J. G. *Int. J. Quantum Chem.* **1996**, *57*, 281–293.
(26) Baerends, E. J.; Ellis, D. E.; Ros, P. *Theor. Chim. Acta* **1972**, *27*, 339–354.

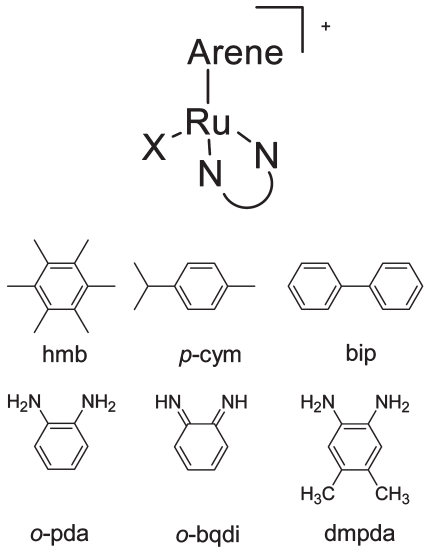

Complex	Arene	N-N	X
1	*p*-cym	*o*-pda	Cl
1a	*p*-cym	*o*-pda	H_2O
2	hmb	*o*-pda	Cl
3	hmb	*o*-bqdi	Cl
4	*p*-cym	*o*-bqdi	I
5	*p*-cym	*o*-bqdi	Br
6	bip	dmpda	Cl
7	*p*-cym	*o*-bqdi	Cl
7a	*p*-cym	*o*-bqdi	H_2O
8	*p*-cym	*o*-pda	I

Figure 1. General structures of complexes studied in this work as PF_6, Cl, or I salts.

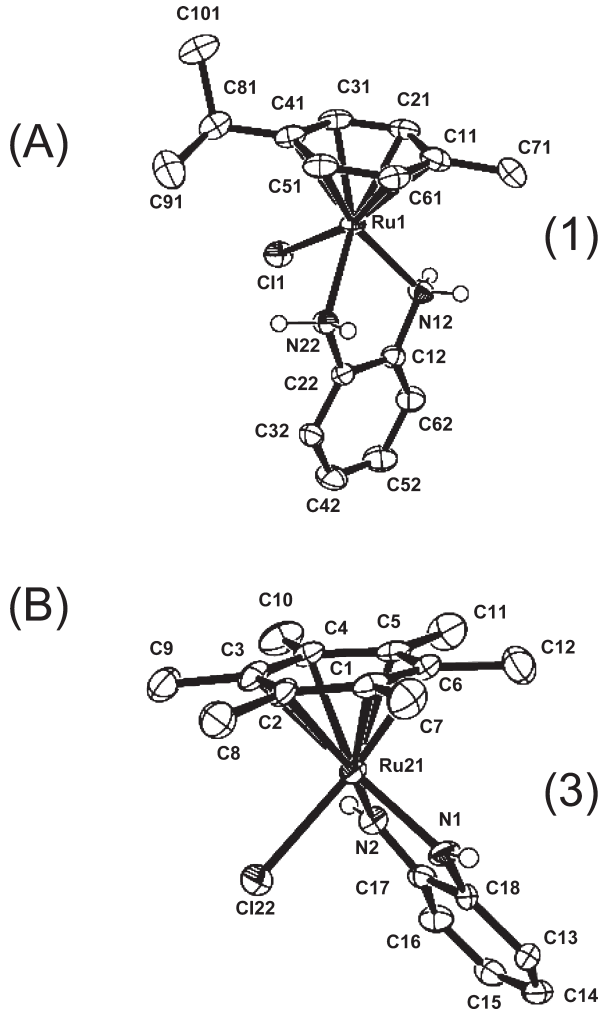

Figure 2. ORTEP diagrams for cations of (A) complex **1** and (B) complex **3PF$_6$** at 50% probability thermal ellipsoids. All hydrogen atoms, apart from NH hydrogen atoms from *o*-pda and *o*-bqdi, have been omitted for clarity.

energies of the separate fragments from that of the whole molecule.

Cytotoxicity. All ruthenium(II) arene complexes synthesized in this work were tested for inhibitory growth activity against A2780 human ovarian cancer and A549 human lung cancer cell lines, using a previously described protocol.[27]

Results

Synthesis and Characterization. The ligands used in this work are shown in Figure 1. Ruthenium(II) arene complexes **1**−**4** and **6** (Figure 1) were synthesized as PF_6, Cl, or I salts, respectively, by the reaction of $[(\eta^6\text{-arene})RuX_2]_2$ (X = Cl or I) and the appropriate chelating ligands, in methanol. The chlorido complex **1** underwent ligand-based oxidation in the presence of ca. 5 mol equiv of KI or KBr in methanol, to afford the diimine iodido and bromido complexes **4** and **5**, respectively. The synthesized complexes **1**−**4** and **6** were fully characterized by ^{1}H NMR and CHN analysis. In addition, complexes **1** and **3**−**6** were characterized by ESI-MS. The elemental analysis of complex **2** suggested that it contained a mixture of counteranions PF_6^- and Cl^- in a 4:1 ratio. Complex **5** was characterized only by ^{1}H NMR and ESI-MS because the yield was low. The synthesis of complex **1** as a BF_4 salt was reported previously.[28] A simplified procedure that leads to isolation of the PF_6 salt is reported here.

All ruthenium(II) imine complexes synthesized in this work (complexes **3**−**5**) exhibited a characteristic broad singlet imine NH resonance at low field (ca. δ 14−15) in ^{1}H NMR spectra from DMSO-d_6 solutions (e.g., δ 14.68 for complex **4**; Figure S1 in the Supporting Information). For all ruthenium(II) amine complexes studied here (**1**, **2**, and **6**), a characteristic doublet amine NH_2 resonance was observed at ca. δ 6−8.

The X-ray crystal structures of **1** and **3** were determined and are shown in Figure 2. The crystallographic data are listed in Table 1 and selected bond lengths and angles in Table 2. The crystal structures of complexes **1** and **3** show the typical pseudo-octahedral "piano-stool" geometry. The "seat" of the stool (π-bonded arene) occupies three coordination sites, and the two nitrogen atoms and chloride fill the remaining three sites.

The distance between the arene centroid and Ru in the *p*-cym complex **1** (1.66 Å) is shorter than that in the hmb

(27) Dougan, S. J.; Melchart, M.; Habtemariam, A.; Parsons, S.; Sadler, P. J. *Inorg. Chem.* **2007**, *46*, 10882–10894.

(28) Govindaswamy, P.; Mozharivskyj, Y. A.; Kollipara, M. R. *Polyhedron* **2004**, *23*, 3115–3123.

Table 1. X-ray Crystal Structure Data for Complexes **1** and **3PF$_6$**

	1	**3**
formula	$C_{16}H_{22}ClF_6N_2PRu$	$C_{18}H_{24}ClF_6N_2PRu$
molar mass	523.85	549.89
cryst syst	orthorhombic	monoclinic
cryst size/mm	0.48 × 0.19 × 0.08	0.35 × 0.14 × 0.06
space group	*Pna*21	*P*121/*c*1
crystal	orange/needle	red/plate
a/Å	10.6876(4)	12.7647(6)
b/Å	17.0748(8)	10.8910(5)
c/Å	10.8625(5)	15.8629(7)
α/deg	90	90
β/deg	90	113.431(3)
γ/deg	90	90
T/K	150(2)	150
Z	4	4
R [$F > 4\sigma(F)$][a]	0.0340	0.0407
R_w[b]	0.0838	0.0948
GOF[c]	1.056	0.6189
Δρ max, min/e Å^{-3}	0.893, −0.450	1.39, −1.31

[a] $R = \sum||F_o| - |F_c||/\sum|F_o|$. [b] $R_w = [\sum w(F_o^2 - F_c^2)^2/\sum wF_o^2)]^{1/2}$. [c] GOF $= [\sum w(F_o^2 - F_c^2)^2/(n-p)]^{1/2}$, where n = number of reflections and p = number of parameters.

Table 2. Selected Bond Lengths (Å) and Angles (deg) for Complexes **1** and **3PF$_6$**

bond/angle	**1**	**3**
Ru−Cl	2.4039(8)	2.3936(13)
Ru−N12/N2	2.156(2)	2.025(4)
Ru−N22/N1	2.141(2)	2.033(4)
Ru−C11/C1	2.188(4)	2.263(4)
Ru−C21/C2	2.195(4)	2.253(4)
Ru−C31/C3	2.166(4)	2.252(4)
Ru−C41/C4	2.207(4)	2.245(5)
Ru−C51/C5	2.163(4)	2.176(5)
Ru−C61/C6	2.186(4)	2.175(5)
N22/N2−Ru−N12/N1	76.18(9)	75.06(15)
N12/N1−Ru−Cl	86.02(8)	87.90(11)
N22/N2−Ru−Cl	83.56(8)	86.71(11)

complex **3PF$_6$** (1.71 Å). The Ru−Cl bond lengths in these two chloridoruthenium(II) complexes are significantly different, with values of 2.4039(8) Å for **1** and 2.3936(13) Å for **3PF$_6$**. In complex **3PF$_6$**, which contains *o*-bqdi as a chelating ligand, the Ru−N distances are significantly shorter [2.033(4) and 2.025(4) Å] than those in the diamine complex **1** [2.141(2) and 2.156(2) Å].

The C−C and C−N bond distances of *o*-pda in complex **1**, and *o*-bqdi in complex **3PF$_6$**, are shown in Figure 3. It can be seen that the C−C bond lengths of *o*-bqdi from **3PF$_6$** are in the range 1.35−1.44 Å, consistent with the presence of C−C single [average 1.440(6) Å] and C=C double [average 1.347(6) Å] bonds. All C−C bond lengths of *o*-pda from **1** are very similar (1.37−1.41 Å), average 1.387(5) Å. The C−N bonds of *o*-bqdi are significantly shorter [1.295(5) and 1.300(6) Å] compared to those of *o*-pda [1.448(4) and 1.452(4) Å]. The observed differences in the C−C and C−N bond lengths can be diagnostic for the assignment of the oxidation state of the chelating ligand.

Ligand-Based Oxidation. Complex **1** is formed as a product of the reaction of the dimer ([(η^6-*p*-cym)RuCl$_2$]$_2$) with *o*-pda, at ambient temperature in air and with methanol as a solvent. Complex **2**, however, was prepared in methanol from the reaction of [(η^6-hmb)RuCl$_2$]$_2$ with *o*-pda, under an argon atmosphere at ambient temperature. When the preparation of **2** was attempted under the same reaction conditions as those of **1** (in air), the result was the formation of a mixture. The ^{1}H NMR spectrum in DMSO-d_6 showed a mixture containing complexes with the reduced diamine ligand *o*-pda (**2**) and the oxidized diimine ligand [(η^6-hmb)Ru(*o*-bqdi)Cl]$^+$ (**3**) in a 1:1 ratio, indicating that changing the arene from *p*-cym to hmb has made *o*-pda more sensitive toward ligand-based oxidation in the presence of molecular oxygen from air.

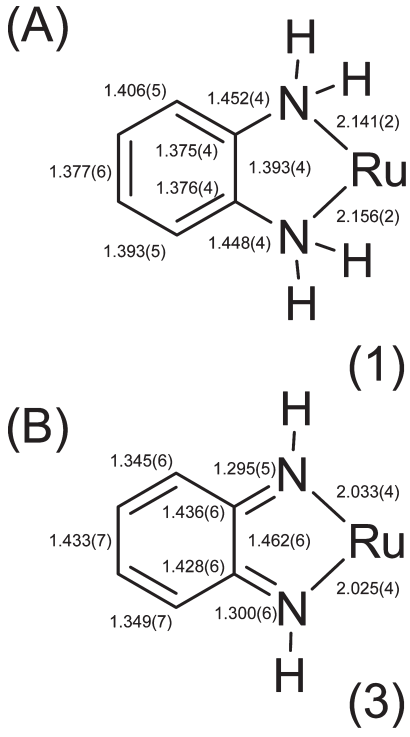

Figure 3. Bond distances for (A) Ru^{II}(*o*-pda) unit of complex **1** and (B) Ru^{II}(*o*-bqdi) unit of complex **3PF$_6$**.

The extent of ligand-based oxidation in **1** and the formation of [(η^6-*p*-cym)Ru(*o*-bqdi)Cl]$^+$ (**7**) in methanol was followed by UV−vis spectroscopy. The data were fitted to the appropriate equation for pseudo-first-order kinetics, giving $k_{obs} = (10 \pm 0.2) \times 10^{-3}$ min^{-1} and $t_{1/2}$ = 68 min. This is ca. 2 times slower than that observed for ligand-based oxidation of the same complex in the presence of 1 mol equiv of KI [$k_{obs} = (24 \pm 0.2) \times 10^{-3}$ min^{-1}; $t_{1/2}$ = 29 min]. The formation of **7** and **4** was confirmed by ESI-MS (for complex **7**: calcd, *m*/*z* 376.9; found, *m*/*z* 377.2; for complex **4**: calcd, *m*/*z* 468.3; found, *m*/*z* 468.9) and by ^{1}H NMR spectroscopy (for complex **7**; Figure 4). The resonances of the aromatic protons of *p*-cym in **7** (two doublets at 6.00 and 6.23 ppm) are shifted to lower field, compared to those of complex **1** (two doublets at 5.56 and 5.76 ppm).

Initially, the UV−vis spectrum of **1** in methanol showed no bands in the visible region; new bands appeared after 5 min at 248, 357, 485, and 690 nm, which increased in intensity with time and are assigned to **7**.

Aquation. Complex **3** underwent relatively fast hydrolysis, $k_{obs} = (92.5 \pm 1.36) \times 10^{-3}$ min^{-1} and $t_{1/2}$ = 7.49 min (Figure 5). The presence of the aqua adduct was confirmed by ESI-MS. The ion peak observed at *m*/*z* 369.7 is assignable to [(η^6-hmb)Ru(*o*-bqdi)H$_2$O]$^{2+}$ after loss of the aqua ligand and a proton (calcd *m*/*z* 369.4 for [(η^6-hmb)Ru(*o*-bqdi)H$_2$O]$^{2+}$–H$_2$O–H$^+$).

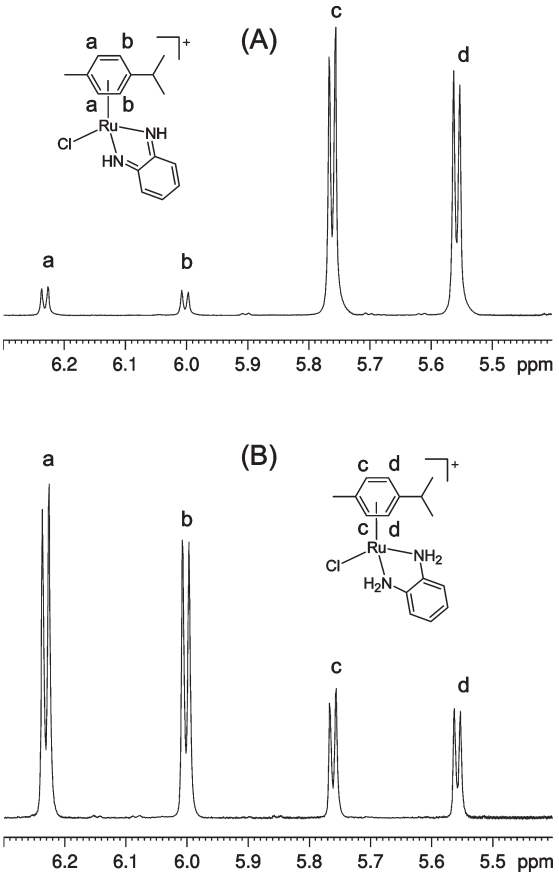

Figure 4. Low-field region of the ^{1}H NMR spectrum of complex **1** in MeOH-d_4: (A) 10 min after dissolution; (B) 4 h after dissolution.

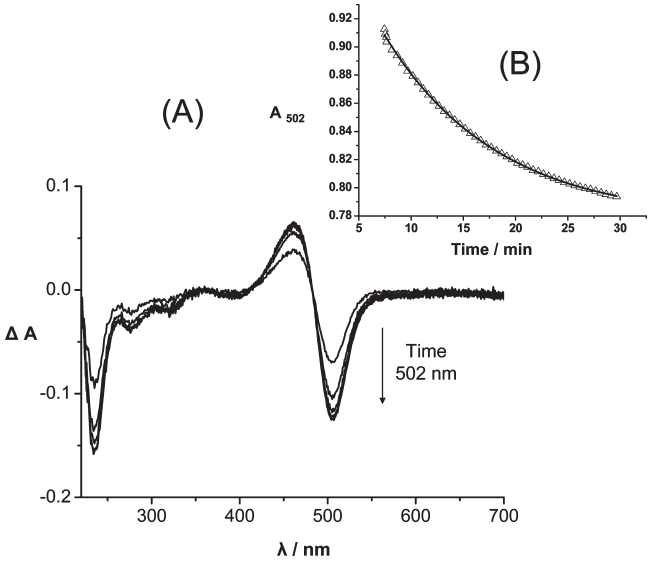

Figure 5. Hydrolysis studies of **3** at 310 K. (A) UV−vis difference spectrum showing that the largest change in absorbance occurs at 502 nm. (B) Change in absorbance at 502 nm over 30 min during the aquation of **3**, from which the kinetic data were derived.

The ^{1}H NMR spectrum of **1** in D_2O after 2 h showed peaks consistent with the presence of four species, corresponding to the chlorido species **1** (5%) and **7** (9%), together with peaks for the aqua adducts $[(\eta^6\text{-}p\text{-cym})\text{Ru}(o\text{-pda})\text{H}_2\text{O}]^{2+}$ (**1a**, 38%) and $[(\eta^6\text{-}p\text{-cym})\text{Ru}(o\text{-bqdi})\text{H}_2\text{O}]^{2+}$ (**7a**, 48%; Figure 6). This is consistent with the

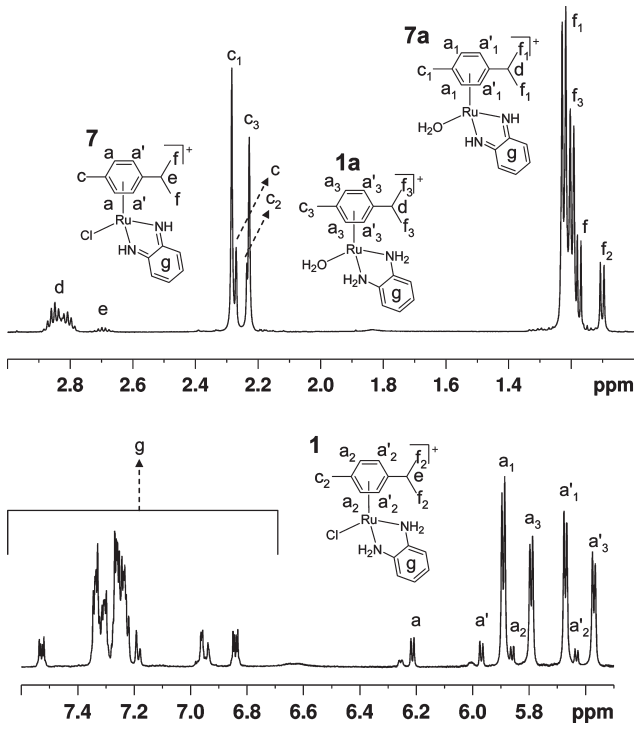

Figure 6. ^{1}H NMR spectrum of complex **1** in D_2O, 2 h after dissolution, showing the formation of **7** and the formation of aqua adducts of both chlorido species (**1a** and **7a**).

formation and an increase in the concentration of the aqua adducts with time. The ESI-MS spectrum of the same solution in D_2O also showed ion peaks that are consistent with the presence of the four species. The peaks corresponding to the two aqua adducts **1a** and **7a** (calcd for $\{\mathbf{1a}\text{-}H_2O\text{–}D\}^+$, m/z 345.4; found, m/z 345.5; calcd for $\{\mathbf{7a}\text{-}H_2O\text{–}D\}^+$, m/z 341.4; found, m/z 341.5; in which the NH protons of *o*-pda and *o*-bqdi exchanged with D) overlapped, but a close analysis showed that there were two sets of peaks. The less intense peaks corresponding to two chlorido species **1** and **7** (Figure 7) were still present in solution, again overlapped (calcd for **1**, with ND_2, m/z 383.0; found, m/z 383.5; calcd for **7**, with ND, m/z 379.1; found, m/z 379.4). Thus, complex **1** in D_2O undergoes hydrolysis as well as ligand-based oxidation, leading to the formation of **1a**, **7**, and **7a**. The formation and increase in the intensity of bands at 251, 350, 468, and 686 nm in the UV−vis spectrum of **1** in water over 1 h is attributable to ligand-based oxidation.

o-bqdi complexes **3** and **4** in water show similar bands in their UV−vis spectra: at 224, 350, 502, and 678 nm for **3** and at 260, 397, 493, and 680 nm for complex **4** (Figure S2 in the Supporting Information). Complex **4** did not undergo hydrolysis over a period of 24 h.

The appearance and increase in the intensity of bands at 251, 347, 475, and 662 nm in the UV−vis spectrum of **6** in water over 1 h suggested that ligand-based oxidation had occurred, as the species formed absorbed at wavelengths similar to those of complexes **3** and **4**. In the ^{1}H NMR spectrum obtained 10 min after dissolution of **6** in D_2O, peaks for free biphenyl were observed (Figure S3 in the Supporting Information), indicating ca. 5% arene loss from the complex.

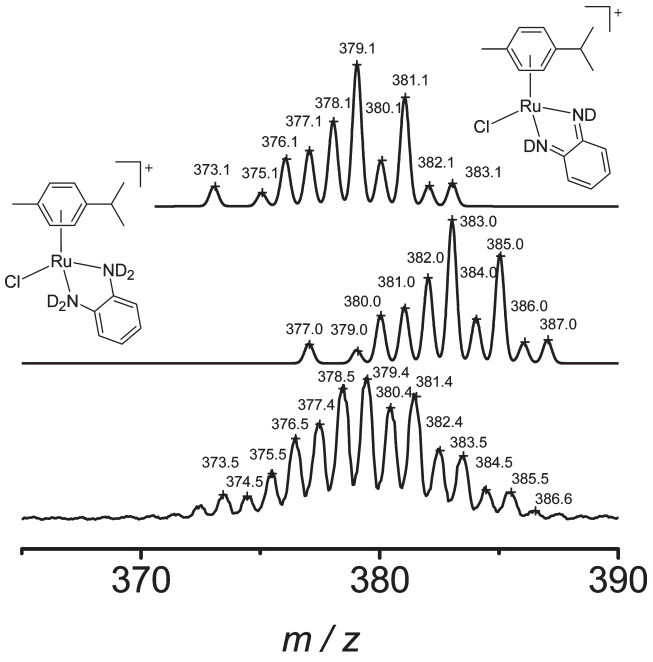

Figure 7. ESI-MS spectrum of a D_2O solution of complex **1** (lowest spectrum) and calculated isotopic patterns (middle and upper spectra) showing that the observed spectrum corresponds to the overlap of two species, intact complex **1** (where the NH protons have been substituted by deuterium) and its oxidized form **7** (again with ND, instead of NH).

Reaction with GSH. UV−vis spectra of **4** in water, in the presence of 15 mol equiv of GSH, showed the complete disappearance of the bands corresponding to **4** after 1 h and the appearance of an isosbestic point at 294 nm (Figure 8). This indicated the reduction of *o*-bqdi to *o*-pda and the formation of **8**, as confirmed by ESI-MS (calcd, *m*/*z* 470.3; found, *m*/*z* 470.9). The resulting colorless solution became purple after standing for 72 h, and the UV−vis spectrum of this solution was identical with that of complex **4** in water.

The ^{1}H NMR spectrum of the diimine complex **4** in D_2O in the presence of 15 mol equiv of GSH showed peaks at 3.30 (d of d) and 3.00 ppm (d of d, overlapped with the peaks of GSH in the same region, two d of d at 2.95 and 2.98 ppm), corresponding to the β-CH_2 protons of GSSG. This suggested that oxidation of GSH to GSSG had occurred.[29] The intensity of these peaks increased with time.

No GSH adduct of **4** in an aqueous solution was detectable by ESI-MS. In negative-ion mode, ion peaks corresponding to $\{GSSG-H\}^-$ (calcd, *m*/*z* 611.2; found, *m*/*z* 611.1) and GS^- (calcd, *m*/*z* 305.1; found, *m*/*z* 304.9) were observed, confirming the formation of GSSG. Further confirmation of the origin of the peak at *m*/*z* 304.9 was achieved by fragmentation studies. The MS/MS spectrum of this peak showed fragmentation peaks consistent with the presence of a glutathionyl unit.[30]

Computation. The optimized geometries of the 2+ cations $[(\eta^6\text{-}p\text{-cym})Ru(o\text{-pda})(9\text{-EtG-}N7)]^{2+}$ (**1EtG**) and $[(\eta^6\text{-hmb})Ru(o\text{-bqdi})(9\text{-EtG-}N7)]^{2+}$ (**3EtG**) are shown in Figure 9. A hydrogen bond of 1.69 Å was formed between O6 of 9-EtG and the NH proton (H_a) of *o*-pda

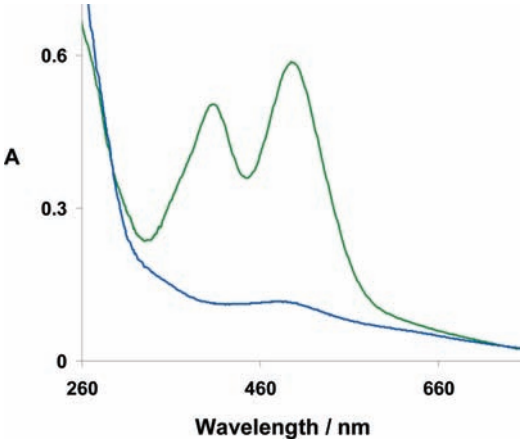

Figure 8. UV−vis spectra of complex **4** in water 5 min after dissolution (top spectrum) and 1 h after the addition of 15 mol equiv of GSH (bottom spectrum) showing the disappearance of the bands in the visible region and the isosbestic point at 294 nm, indicating the reduction of *o*-bqdi to *o*-pda and the formation of **8**.

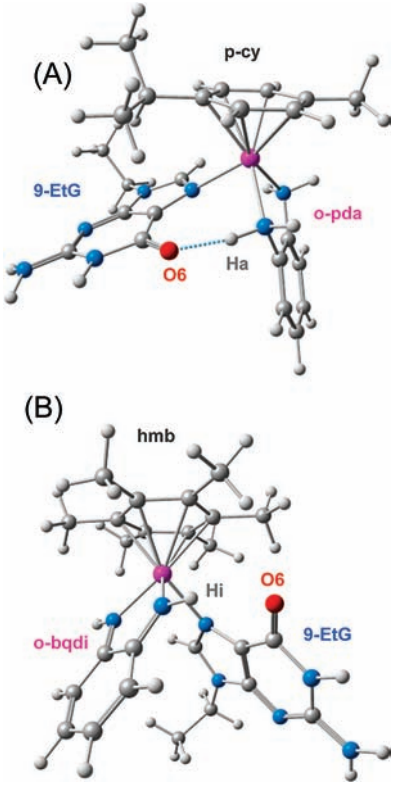

Figure 9. Optimized geometries of 9-EtG adducts of complexes **1** and **3**.

(Figure 9A) in the optimized structure of **1EtG**. The distance between O6 from 9-EtG and H_i from NH of *o*-bqdi (Figure 9B) in the optimized structure of **3EtG** is 2.22 Å. The binding energy of 9-EtG to the metal fragment in **1EtG** is −328.1 kJ/mol, which is 23.8 kJ/mol lower than the corresponding value for **3EtG** (−304.3 kJ/mol).

The Veronoi deformation density (VDD) method for computing atomic charges has been previously used for transition metals such as chromium and iron in complexes $Cr(CO)_6$ and $Fe(CO)_5$.[31] VDD charges on

(29) Nakayama, T.; Isobe, T.; Nakamiya, K.; Edmonds, J. S.; Shibata, Y.; Morita, M. *Magn. Reson. Chem.* **2005**, *43*, 543–550.

(30) Dieckhaus, C. M.; Fernandez-Metzler, C. L.; King, R.; Krolikowski, P. H.; Baillie, T. A. *Chem. Res. Toxicol.* **2005**, *18*, 630–638.

(31) Guerra, C. F.; Handgraaf, J. W.; Baerends, E. J.; Bickelhaupt, F. M. *J. Comput. Chem.* **2003**, *25*, 189–210.

Table 3. IC_{50} Values for Ru^{II} Complexes Synthesized in This Work Against the A2780 Human Ovarian and A549 Human Lung Cancer Cell Lines

complex		IC_{50} (μM)	
		A2780	A549
(η^6-*p*-cym)Ru(*o*-pda)Cl]PF_6	**1**	11[a]	> 100
[(η^6-hmb)Ru(*o*-pda)Cl]PF_6[b]	**2**	> 50[c]	ND[d]
[(η^6-hmb)Ru(*o*-bqdi)Cl]Cl	**3**	> 100	> 100
[(η^6-*p*-cym)Ru(*o*-bqdi)I]I	**4**	> 100	> 100
[(η^6-bip)Ru(dmpda)Cl]PF_6	**6**	49	> 100

[a] The IC_{50} data for **1** with A2780 human ovarian cancer cells were reported previously.[7] [b] Complex **2** is unstable in solution toward the ligand-based oxidation and is likely to be present in the test medium as the oxidized product **3**. [c] Complex **2** was not tested for activity above 50 μM, whereas the other complexes were tested for activity up to 100 μM. [d] ND = not determined.

ruthenium in **1EtG** and **3EtG** revealed differences in the electron density on the metal. In complex **1EtG**, the atomic charge on ruthenium is +0.25 au and it is +0.31 au in complex **3EtG**, a difference of 0.06 au.

Cytotoxicity. None of the complexes tested (**1**, **3**, **4**, or **6**) showed activity against A549 human lung cancer cells (IC_{50} > 100 μM; Table 3). Complex **1** containing *o*-pda as a chelating ligand showed the highest activity against A2780 human ovarian cells (IC_{50} = 11 μM). In contrast, complexes containing the oxidized form of *o*-pda (*o*-bqdi) as a chelating ligand (complexes **3** and **4**) showed no activity (IC_{50} > 100 μM) against the A2780 cell line. Complex **6**, containing dmpda as a chelating ligand, showed moderate activity against A2780 cells (IC_{50} = 49 μM). Although the activity of complex **5** was not determined, it would be predicted to be inactive. It is likely that both bromido and iodido ligands in these complexes would be substituted by chloride in an extracellular biological media where the concentration of chloride is ca. 104 mM, so that these complexes would in any case act as prodrugs.[32] The IC_{50} of complex **2** toward A2780 cells was found to be >50 μM.

Discussion

In this work, we have investigated the oxidation of the diamine ligand *o*-pda to its diimino form *o*-bqdi in ruthenium(II) arene complexes and its effect on cytotoxicity toward cancer cells. We have also investigated the nature of the oxidation process as a function of changes in the electronic properties of the arene and substitution of the halide ligand.

The *o*-bqdi(imino)$_2$ ligand has been found to exist in solution[33] but has never been isolated in any form. For example, *o*-bqdi was observed as a product from the reaction of *o*-pda with PbO_2, giving a deep-red color in organic solvents.[34] This reactive ligand can be stabilized by coordination to metal ions. For tris(α-diimine)iron(II) complexes, theoretical considerations have shown that a significant π-electron backdonation takes place in the ground state, and as a result, unusually stable Fe^{II} complexes are formed.[35] Similarly, low-spin d^6 Ru^{II} complexes containing *o*-bqdi as the α-diimine ligand are particularly stable.[36] Ru^{II} complexes containing *o*-bqdi have previously been synthesized[36] and structurally characterized.[37−39] The oxidation of *o*-pda and the formation of *o*-bqdi have an effect on the overall physical and chemical properties of ruthenium(II) arene complexes, including absorption spectra, hydrolysis rates, and cytotoxicity.

Synthesis and Characterization. Complex **2** contains a strong electron-donating arene (hmb), and in methanol, the absence of oxygen is necessary to prevent the formation of the *o*-bqdi species. On the other hand, the presence of the relatively less electron-donating arene (*p*-cym) in **1** makes this complex less sensitive to oxidation. Therefore, the oxidation of *o*-pda and the formation of an "electron-poor" ligand (*o*-bqdi) are favored in complexes where the metal center is more "electron-rich". The stability of the "electron-poor" *o*-bqdi ligand in $[Ru^{II}(bpy)_2(o\text{-bqdi})]^{2+}$ has been ascribed to its π-accepting ability in conjunction with a low-spin "electron-rich" Ru^{II} as a π donor.[37] In contrast, rhenium complexes with oxidation states up to 7+ containing $(o\text{-pda})^{2-}$ ligands contain a combination of an "electron-rich" diamine ligand and an "electron-poor" metal ion.[40]

The ^{1}H NMR resonances of the NH protons from *o*-bqdi appeared in the low-field region of the spectra (ca. δ 14−15) compared to those of the NH_2 protons from *o*-pda (ca. δ 6−8). The NH proton resonances from *o*-bqdi have been observed at 11.96 ppm for $[Ru(o\text{-bqdi})_3]^{2+}$ and at 7.0 ppm for the aromatic protons from the same chelating ligand.[36] This chemical shift is close to that observed for the aromatic protons of *o*-bqdi in complexes **3**−**5** (ca. δ 7.1). The ^{1}H NMR resonances of NH (*o*-bqdi) protons of $[Ru(o\text{-pda})(o\text{-bqdi})_2]^{2+}$ have different chemical shifts at δ 11.20 and 14.24, as a result of the different environments of these protons.[41]

The significantly shorter Ru−Cl bond in the crystal structure of $\mathbf{3PF_6}$ compared to that of **1** can be attributed to the strong π-acceptor *o*-bqdi in $\mathbf{3PF_6}$. As a consequence of the reduced electron density on the ruthenium center, the negatively charged chlorido ligand is bound strongly. It has been found that the π-accepting ability of the ligand L in $[Ru(NH_3)_nL]^{2+}$, where n = 4 or 5 and L = pyrazine (pyz), 2,2′-bipyridine (bpy), imidazole (im), or *o*-bqdi, follows the order o-bqdi ≫ pyz > bpy > im.[42] Therefore, the effective charge on ruthenium in *o*-bqdi complexes is the highest in the series. The presence of significantly shorter Ru−N bonds in the crystal structure of $\mathbf{3PF_6}$ (average bond length of 2.029(4) Å; Table 2) compared to those of **1** (average bond length of 2.148(2) Å; Table 2) again is consistent with the strong π-acceptor ability of *o*-bqdi. Structural parameters obtained from several

(32) Kennedy, R. S.; Konok, G. P.; Bounous, G.; Baruchel, S.; Lee, T. D. G. *Anticancer Res.* **1995**, *15*, 2643–2649.
(33) Christoph, G. G.; Goedken, V. L. *J. Am. Chem. Soc.* **1973**, *95*, 3869–3875.
(34) Willstatter, R.; Pfannenstiel, A. *Ber. Deutsch. Chem. Ges.* **1905**, *38*, 2348–2352.
(35) Ito, T.; Tanaka, N.; Hanazaki, I.; Nagakura, S. *Bull. Chem. Soc. Jpn.* **1968**, *41*, 365–373.
(36) Warren, L. F. *Inorg. Chem.* **1977**, *16*, 2814–2819.
(37) Belser, P.; Von Zelewsky, A.; Zehnder, M. *Inorg. Chem.* **1981**, *20*, 3098–3103.
(38) Milliken, B.; Borer, L.; Russell, J.; Bilich, M.; Olmstead, M. M. *Inorg. Chim. Acta* **2003**, *348*, 212–216.
(39) Rusanova, J.; Rusanov, E.; Gorelsky, S. I.; Christendat, D.; Popescu, R.; Farah, A. A.; Beaulac, R.; Reber, C.; Lever, A. B. P. *Inorg. Chem.* **2006**, *45*, 6246–6262.
(40) Danopoulos, A. A.; Wong, A. C. C.; Wilkinson, G.; Hursthouse, M. B.; Hussain, B. *Inorg. Chem.* **1990**, 315–331.
(41) Cheng, H. Y.; Peng, S. M. *Inorg. Chim. Acta* **1990**, *169*, 23–24.
(42) Baranovski, V. I.; Sizova, O. V. *Chem. Phys. Lett.* **1999**, *315*, 130–134.

reported crystal structure determinations can be used to assign the oxidation levels of the chelating ligand and allow comparisons to be made.[43] The lengths of the C=N [average 1.298(8) Å] and C=C [average 1.347(6) Å] bonds of *o*-bqdi in complex **3PF$_6$** (Figure 3) are consistent with their assignments as localized double bonds and are close to the C=N [average 1.300(8) Å] and C=C [average 1.339(9) Å] bond lengths observed in $[(o\text{-bqdi})_3Fe^{II}]^+$.[43] The lengths of the C−C bonds of *o*-bqdi in the crystal structures of $[(o\text{-bqdi})_3Fe^{II}]^+$ [average 1.437(10) Å] and **3PF$_6$** [average 1.440(6) Å; Figure 3] are very similar. In the crystal structure of complex **3PF$_6$**, the Ru−arene centroid distance is 1.71 Å, whereas for $[(\eta^6\text{-hmb})Ru(en)Cl]^+$, it is 1.67 Å.[44] This indicates slightly weaker π-back-bonding between ruthenium and the arene in complex **3PF$_6$**, in which more electron density is withdrawn from the metal by *o*-bqdi than by hmb.

All of the *o*-bqdi complexes studied (**3**, **4**, **7**, and the oxidation product of **6**) exhibit two metal-to-ligand charge-transfer (MLCT) bands in UV−vis spectra (in the ranges of 468−502 and 224−260 nm in water or methanol). The low- and high-energy MLCT transitions are assigned to Ru $4d^6 \rightarrow \pi_1^*$ (*o*-bqdi) and Ru $4d^6 \rightarrow \pi_2^*$ (*o*-bqdi) transitions by analogy with the assignment of the bands at 480 and 255 nm for $[Ru^{II}(edta)(o\text{-bqdi})]^{2-}$ [45] and at 470 and 258 nm for $[Ru^{II}(NH_3)_4(o\text{-bqdi})]^{2+}$.[46] The d−d bands for the chlorido complexes (**3**, **7**, and the oxidation product of **6**) in water or methanol appeared in the range of 350−360 nm, while for the iodido complex **4** (Figure S2 in the Supporting Information), the same transition occurs at lower energy (397 nm). π-Donation decreases in the order I > Br > Cl for $(Cp)Ru(PH_3)X$ complexes, where X = I, Br, or Cl.[47] This should make the d−d transition higher in energy for chloridoruthenium(II) compared to the iodido complexes, resulting in hypsochromic (blue) shifts in the UV−vis spectrum.[48] All of the complexes show a band in the UV−vis spectra in the region of 662−690 nm in water or methanol. This low-intensity band is similar to that observed for $[Ru^{II}(edta)(o\text{-bqdi})]^{2-}$ at ca. 575 nm in aqueous solution; its origin is unclear but may be associated with the low-energy MLCT transition.[45]

Ligand-Based Oxidation. Methanol and water solutions of **2** are more sensitive to molecular oxygen (from air) in contrast to solutions of **1** because of the difference in the arene (vide infra). These solutions react with dioxygen to yield intensely purple products. In the ^{1}H NMR spectrum of **1** in MeOH-d_4 (Figure 4), the formation of **7** was detected. The intensity of the peaks corresponding to the protons of **7** increased with time, indicating an increase in the concentration of the oxidized product (**7**). After 4 h, the ratio of **7**/**1** was 3:1 (Figure 4B). For **7**, the aromatic *p*-cym ^{1}H NMR peaks are shifted to low field because of the deshielding of these protons by the π-accepting *o*-bqdi ligand (6.00 and 6.23 ppm). During aquation of **1**, the formation of **7** was detected by UV−vis spectroscopy. Isosbestic points were not apparent, indicating a multistep reaction pathway. Similar observations have been reported by Kockerbauer and Bednarski for the ligand-based oxidation of $(o\text{-pda})Pt^{II}Cl$ complexes in water.[49]

The ease with which the hmb complex **2** is oxidized compared to the *p*-cym complex **1** is related to the increased number of electron-donating substituents on the arene in **2**. The presence of electron-donating alkyl groups on the arene has been found to strengthen the Ru−arene bond[50] and effectively increase the electron density on the ruthenium center. The same effect is observed when substituting Cl with the less electronegative Br or I (in complexes **4** and **5**) ligand, resulting in less polarized Ru−Br/I bonds. Hence, the increased electron density on the ruthenium center favors the formation of the oxidized diimine complexes **4** and **5**.

Simultaneous oxidation and arene loss occurred during the aquation of **6**, even though the replacement of *p*-cym and hmb as the arene by the more electron-deficient bip[51,52] should make the ruthenium center even more acidic, stabilize the chelating ligand and make the oxidation less favorable. Arene loss (detected in ^{1}H NMR in D_2O; Figure S3 in the Supporting Information) may arise from the oxidation of the chelating ligand, giving a relatively strong π acceptor (dmbqdi), which competes with bip (relatively weak π acceptor) for electrons on ruthenium. This destabilizes the Ru−arene bond through the lack of π-back-donation, resulting in dissociation of the arene from Ru. Arene loss was not observed for the other complexes studied here.

Hydrolysis. The ^{1}H NMR spectrum of **1** in D_2O (Figure 6) showed the formation of the oxidized product **7**, as well as aqua adducts **1a** and **7a**. Thus, complex **1** hydrolyzes as it undergoes ligand-based oxidation (vide infra).

For Ru^{II} complexes, the presence of a π-acceptor chelating ligand decreases the rate of hydrolysis compared to that of the en analogues,[27] by decreasing the electron density on ruthenium and reducing Cl^- lability. Thus, the hydrolysis of complex **3** was found to be 17 times slower than that previously observed for $[(\eta^6\text{-hmb})Ru(en)Cl]^+$.[44] The iodido complex **4** was found not to undergo hydrolysis. The absence of hydrolysis for the iodido azopyridine complexes $[(\eta^6\text{-arene})Ru(azpy)I]^+$, where arene = bip or *p*-cym and azpy = *N*, *N*-dimethylphenyl- or hydroxyphenylazopyridine, has also been reported.[53]

Reaction with GSH. GSH is the primary cellular antioxidant and is present in cells in concentrations of ca.

(43) Peng, S. M.; Chen, C. T.; Liaw, D. S.; Chen, C. I.; Wang, Y. *Inorg. Chim. Acta* **1985**, *101*, L31–L33.
(44) Wang, F.; Habtemariam, A.; van der Geer Erwin, P. L.; Fernandez, R.; Melchart, M.; Deeth Robert, J.; Aird, R.; Guichard, S.; Fabbiani Francesca, P. A.; Lozano-Casal, P.; Oswald Iain, D. H.; Jodrell Duncan, I.; Parsons, S.; Sadler Peter, J. *Proc. Natl. Acad. Sci. U.S.A.* **2005**, *102*, 18269–18274.
(45) Rein, F. N.; Rocha, R. C.; Toma, H. E. *Electrochem. Commun.* **2002**, *4*, 436–441.
(46) Metcalfe, R. A.; Lever, A. B. P. *Inorg. Chem.* **1997**, *36*, 4762–4771.
(47) Reddy, A. R.; Ranjini, A. S.; Das, P. K.; Samuelson, A. G. *Inorg. Chim. Acta* **2007**, *360*, 2778–2782.
(48) Bickford, C. C.; Johnson, T. J.; Davidson, E. R.; Caulton, K. G. *Inorg. Chem.* **1994**, *33*, 1080–1086.
(49) Kockerbauer, R.; Bednarski, P. J. *J. Inorg. Biochem.* **1996**, *62*, 281–298.
(50) Dadci, L.; Elias, H.; Frey, U.; Hoernig, A.; Koelle, U.; Merbach, A. E.; Paulus, H.; Schneider, J. S. *Inorg. Chem.* **1995**, *34*, 306–315.
(51) Peacock, A. F. A.; Parsons, S.; Sadler, P. J. *J. Am. Chem. Soc.* **2007**, *129*, 3348–3357.
(52) Hung, Y.; Kung, W. J.; Taube, H. *Inorg. Chem.* **1981**, *20*, 457–463.
(53) Dougan, S. J.; Habtemariam, A.; McHale, S. E.; Parsons, S. *Proc. Natl. Acad. Sci. U.S.A.* **2008**, *105*, 11628–11633.

2−10 mM. In many cases, cancer cell resistance to drugs is correlated with an increased level of GSH in cancer cells compared to normal cells.[32] For this reason, reactions of ruthenium(II) arene complexes with GSH are of particular importance.

The stabilization of the Ru^{II} center by the π-acceptor *o*-bqdi[54] suggests that reduction of *o*-bqdi back to *o*-pda is not favorable. In the presence of 15 mol equiv of GSH, complex **4** underwent ligand-based reduction to form **8**. In the presence of oxygen (air) in solution, complex **8** is unstable and reoxidizes to **4**. After the solution was left standing for 72 h at 310 K, complete conversion of **8** back to complex **4** was observed, indicating that once all of GSH had been oxidized to GSSG, dissolved oxygen from the air can cause ligand reoxidation and formation of stable complex **4**. Because GSH is present in most cells at millimolar concentrations (vide infra), intracellular reduction of diimine to diamine complexes could provide a route to activation. Because no activity was detected for the diimine complexes against either the ovarian or lung cancer cells tested in this work (Table 3), it would appear that reduction by GSH does not represent an effective activation mechanism in cells, either because of reoxidation by oxygen or because it is too slow.

Computation. The *o*-bqdi ligand in the crystal structure of **3** (Figure 2B) and the optimized structure of **3EtG** (Figure 9B) has a planar geometry, with both NH groups lying in the same plane. This results in the O6 atom of 9-EtG in **3EtG** being further away from the NH protons of *o*-bqdi than from the NH_2 protons of the reduced ligand. The hydrogen bond formed between H_i and O6 is weaker (Figure 9B; 2.22 Å) compared to that formed between an NH proton of *o*-pda and O6 of 9-EtG in **1EtG**. The tetrahedral geometry around the N donors of *o*-pda in **1EtG** (Figure 9A) results in one hydrogen (H_a) pointing toward O6, making the hydrogen bond strong (1.69 Å). The hydrogen bond between H_a and O6 in **1EtG** appears to be stronger than that observed in en complexes of the type $[(\eta^6\text{-arene})Ru(en)(9\text{-EtG-}N7)]^{2+}$, where arene = bip, tetrahydroanthracene (tha), and dihydroanthracene (dha). Hydrogen bonds in ethylenediamineruthenium(II) arene complexes have lengths of, e.g., 1.868 Å for the bip complex, 1.919 Å for the tha complex, and 2.081 Å for the dha complex.[55] The hydrogen bond in **1EtG** is similar in length to that of the NH proton of en and O6 in the energy-minimized structure of $[(\eta^6\text{-}p\text{-cym})Ru(en)(9\text{-EtG-}N7)]^{2+}$ (1.67 Å).[56]

The total bonding energy of 9-EtG in the structure of **1EtG** (−328.1 kJ/mol) is 23.8 kJ/mol lower than the bonding energy of 9-EtG in **3EtG** (−304.3 kJ/mol). This might be attributed largely to the increased stabilization of the 9-EtG adduct of **1** through the stronger hydrogen bond described above. The charge on the metal center in **3EtG** (+0.31 au) is 0.06 more positive than that in **1EtG** (+0.25 au), which is consistent with *o*-bqdi acting as a π acceptor. Considering the role of the arenes, hmb in **3EtG** with six CH_3 substituents on the arene ring would be a stronger electron donor than *p*-cym in **1EtG**. Still the effect of the arene is noticeably smaller compared to the effect of the chelating ligand, and this leaves the ruthenium in complex **3EtG** with a higher positive charge compared to the ruthenium in **1EtG**.

Cytotoxicity. Complexes containing mono- or dimethylated *o*-pda and indan as the arene exhibited good activity, with IC_{50} values of 4 and 14 μM, respectively.[7] The loss of activity for the biphenylarene complex **6**, which contains dimethylated *o*-pda, might arise from dissociation of the bip ligand from the complex (vide infra). For complexes containing *o*-bqdi as the chelating ligand, no activity was observed. This might be related to the reduction in the electron density on ruthenium caused by the presence of the π-acceptor *o*-bqdi; this makes it harder for Cl^- to leave and results in slower hydrolysis or no hydrolysis at all for the iodido complex **4**. The absence of hydrolysis is likely to hinder reactions with DNA, and this might account for the loss of cytotoxic activity. The relatively fast hydrolysis of $[(\eta^6\text{-}p\text{-cym})Ru(en)I]^+$ ($t_{1/2}$ = 12.2 min)[44] is accompanied by the good cytotoxic activity of this complex (IC_{50} = 9 μM against A2780 cells).[5] The inactive complex **3** showed relatively fast hydrolysis and a potential ability to bind to DNA. However, the 9-EtG adduct of **3** was not as stable as the adduct of **1** (vide infra), which might account for its inactivity. The inactivity of complex **2** can be explained by the relative ease with which it is oxidized to give **3**.

Conclusions

Here we have shown, for the first time, that ruthenium(II) arene complexes containing the diamine *o*-pda as a chelating ligand can lose their cytotoxic activity toward cancer cells upon oxidization to give *o*-bqdi diimine complexes. This oxidation can be controlled through changes in the electronic properties of the other ligands (arene and monodentate ligands) in the complex. The ligand-based oxidation can be followed by UV−vis and ^1H NMR spectroscopy, and the oxidation state of the ligand can be distinguished in the X-ray crystal structure. The loss of activity in this series of complexes may be related to the absence of hydrolysis as well as to the formation of the less stable adducts with guanine (9-EtG), which would lead to a weak binding to DNA. Interestingly, the *o*-bqdi complexes can be reduced by the tripeptide GSH but readily undergo reoxidation in air.

Acknowledgment. We thank Oncosence Ltd., ORSAS, University of Edinburgh. and the University of Warwick for financial support for T.B., Emily Jones and Daniel Simpson (Oncosense Ltd.) for cytotoxicity tests, and Sabine van Rijt for the screening of complex **2** against the A2780 cancer cell line. We thank members of EC COST Action D39 for stimulating discussions.

Supporting Information Available: Crystallographic data in CIF format and Figures S1−S3. This material is available free of charge via the Internet at http://pubs.acs.org.

(54) Juestel, T.; Bendix, J.; Metzler-Nolte, N.; Weyhermueller, T.; Nuber, B.; Wieghardt, K. *Inorg. Chem.* **1998**, *37*, 35–43.
(55) Chen, H.; Parkinson, J. A.; Parsons, S.; Coxall, R. A.; Gould, R. O.; Sadler, P. J. *J. Am. Chem. Soc.* **2002**, *124*, 3064–3082.
(56) Gossens, C.; Tavernelli, I.; Rothlisberger, U. *J. Chem. Theory Comput.* **2007**, *3*, 1212–1222.